Magnetic Performance of a Single Phase Induction Motor under Triac-based Voltage Control

CHRISTOS MADEMLIS[1] and ALEX MICHAELIDES[2]

[1]Department of Electrical and Computer Engineering
Aristotle University of Thessaloniki
Thessaloniki, 54 124
GREECE

[2]Vector Fields Ltd,
24 Bankside, Kidlington, Oxford OX5 1JE
UNITED KINGDOM

Abstract: - The magnetic performance of a capacitor-run single-phase induction motor under triac-based voltage control is examined and compared with that accomplished by the nominal voltage supply. The magnetic field is calculated through two-dimensional finite elements in steady state, including the effect of rotor rotation. Selected calculated results are presented and the effect of a non-sinusoidal voltage supply on magnetic performance of the single-phase induction motor is discussed.

Key-Words: - Finite element method, harmonic analysis, magnetic analysis, single phase induction motors, triac control, voltage control drive.

1 Introduction

Single-phase induction motors (SPIMs) are widely used in various domestic and light-duty industrial applications where a three-phase supply is not readily available [1]. Although they are simpler in construction, they are inherently more complex to model and analyze through equivalent circuits. Moreover, the complexity of the model analysis is increased, if a SPIM is excited through a non-sinusoidal voltage. Thus, the finite element approach could be an effective tool for facilitating and expediting SPIMs performance analysis.

In SPIMs, the unbalanced operation lays on the fact that both main and auxiliary stator windings are fed by the same supply unit. The function of the capacitors (i.e. start and running capacitors) is to generate a leading phase current in the auxiliary winding so that the motor can produce a sufficient high starting torque and operate as a balanced two-phase machine. However, the impedance of the auxiliary winding changes considerably from starting to running mode and also depends on the load condition during the period of normal operation [1]. Therefore, symmetrical and balanced operation of a SPIM cannot be ensured through altering the two fixed value capacitors.

Since hundreds of thousands SPIMs are being used in various applications, the interest for cost effective design, high efficiency and high motor performance are of great importance [2]. Specifically, design considerations for improving SPIMs efficiency and performance were presented in [3] and [4]. A dynamic model of an integral-cycle SPIM by properly choosing a stationary *d-q* reference frame was described in [5] and unified approaches to SPIMs analysis were presented in [6] and [7]. A circuit simulation for both qualitative and quantitative analysis of SPIMs with triac-based supply voltage control was given in [8]. A computer simulation of SPIM in motoring, generating and braking modes using two-dimensional finite elements was presented in [9] and a finite element time-harmonic simulation based on the double revolving field theory was developed in [10]. Finally, investigation of harmonic influence and studies for toque performance improvement of SPIMs were conducted in [11] and [12], respectively.

In this paper, the magnetic performance of a SPIM with triac-based voltage control to achieve adjustable speed operation is investigated and compared with that accomplished by the nominal voltage supply. Triac-based voltage controllers tend to introduce harmonics that may reduce motor efficiency and increase torque pulsations, however they satisfy the prerequisites of simplicity, reliability and cost effectiveness for low horsepower rating SPIMs. Also in this paper, modern FEA tools are employed for the modeling of the SPIM. FEA

analysis includes transient simulations and rotor rotation is included to enable accurate simulation analysis of the SPIM unbalance operation, hence alleviating the need for the double revolving theory approach. The driving functions for the finite element motor model are experimentally obtained. Finally, the effect of the non-sinusoidal voltage of the triac-based voltage controller on the SPIM performance was discussed.

2 General Concepts

2.1 Field and Torque Formulations

The steady-state two-dimensional magnetic field diffusion equation is given by

$$-\nabla\left(\frac{1}{\mu}\nabla A_z\right) = J_s - \sigma\frac{\partial A_z}{\partial z} \qquad (1)$$

where μ is the magnetic permeability, σ is the conductivity, and A_z and J_z are the axial components of the magnetic vector potential and the source current density respectively. The instantaneous electromagnetic torque T_e and the rotor angular acceleration $d\omega_r/dt$ (where ω_r is the mechanical angular velocity) are related by

$$T_e = J_r\frac{d\omega_r}{dt} + T_L \qquad (2)$$

where T_L is the load torque and J_r is the rotor and load body inertia.

The finite element solution of the diffusion equation (1) calculates the magnetic field at distinct time steps. The time stepping is automatically adjusted with coupling to the mechanical equation (2) and relative motion between rotor and stator, so that the calculated error is much less the desired tolerance. For the SPIM finite element simulation, the RM module of the commercial software package OPERA from Vector Fields is employed, that provides coupling to voltage driven circuits and allows for rotor rotation under a user- defined mechanical load coupled to the rotor [13].

2.2 Model Description

A SPIM is provided with two stator windings (i.e. main and auxiliary winding) and a squirrel cage rotor. The two windings are wound 90^0 apart along the air gap space. If the two sets of space symmetric windings are excited by a two-phase symmetrical *ac*-voltage, a smooth rotating field will be produced.

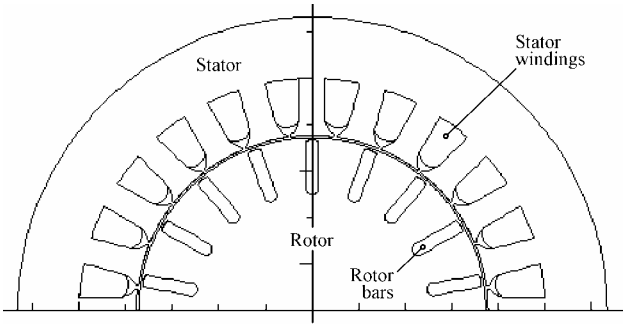

Fig. 1. SPIM cross-section without frame.

TABLE 1
1-HP, 4-POLES SPIM NAMEPLATES AND PARAMETERS

SPIM nameplates	
V_s = 220 V	I_s = 5.6 A
n_r = 1420 rpm	
C_{start} = 150 μF	C_{run} = 25 μF
SPIM parameters	
r_{sm} = 3.2 Ω	r_{sa} = 7.2 Ω
L_{ms} = 0.175 H	
L_{lsm} = 11.5 mH	L_{lsa} = 6.68 mH
r_r' = 2 Ω	L_r' = 10.2 mH

However, the two windings are fed from a common single-phase source. Hence, a capacitor is connected in series with one phase winding (auxiliary winding) in order to generate a leading phase current, so that the motor can produce a sufficiently high starting torque.

The most common SPIM types are split-phase, capacitor-start and capacitor-start-and-run [1], [2]. The split-phase motors have the problem of poor starting torque that is solved by using a capacitor-start in series with the auxiliary winding. The start capacitor may be disconnected after starting by means of a centrifugal switch. In capacitor-start-and-run SPIMs, one more capacitor is permanently connected to the auxiliary winding for improving motor performance.

The cross section of the 4-pole, 1-hp SPIM used in the computations and experiments is shown in Fig. 1. Exploiting model and circuit symmetry in the machine, only one pair of pole pitches was modeled. The field pattern is repeated in the symmetric sections of the machine. The design characteristics of the modeled 1-hp SPIM are recorded in Table 1.

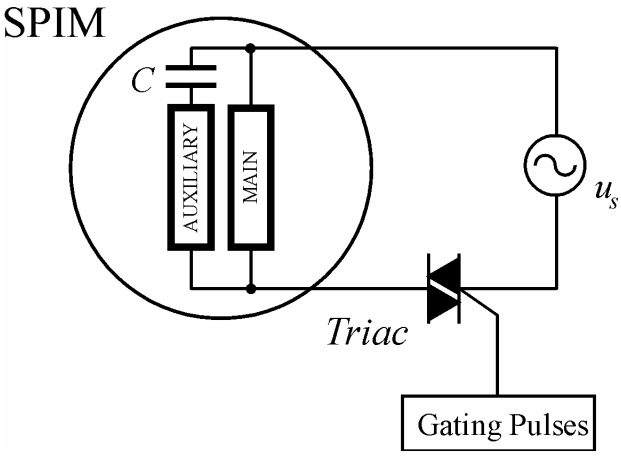

Fig. 2. Block diagram of the triac-based SPIM drive.

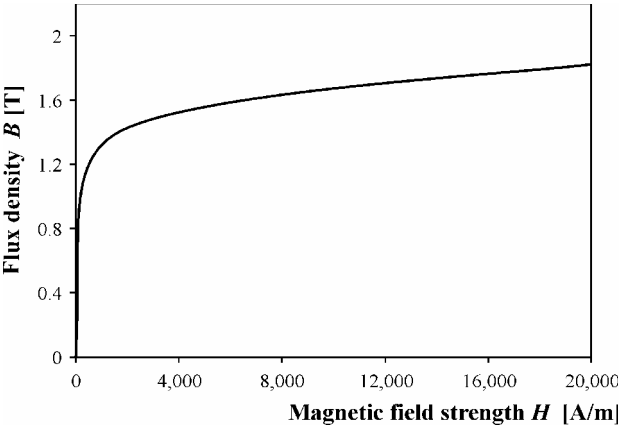

Fig. 3. Magnetization curve and core laminations.

3 System Configuration

To improve the SPIMs performance, power electronic means have been employed increasingly in recent years to achieve adjustable speed operation, in various demanding applications [14], [15]. Although, various PWM control techniques, that exhibit improved performance such as *V/f* control or field-oriented control, have been recently developed for three phase machines [16], the simple triac-based converters are often employed for SPIMs. This is because the complexity and high cost of the newly developed controllers are not justifiable for SPIMs with low horsepower rating. Therefore, a SPIM coupled with a simple, reliable, and cost-effective drive is an ideal solution for most of the commercial and residential applications [2].

The control algorithms for SPIMs can be categorized into phase control and integral-cycle control methods [15]. In the phase control, the effective stator voltage is adjusted by means of a triac-based circuit, which conducts for a portion of half-cycle. In the integral-cycle, the triac is

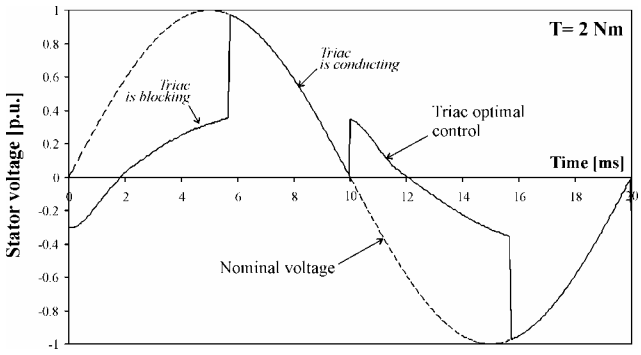

Fig. 4. Experimental stator voltage waveforms (nominal and triac output circuit voltage) used as driving functions for the finite element motor model.

alternately switching on and off the supply voltage for a number of cycles at a time. In integral-cycle systems, less voltage distortion is produced on the ac supply, compared to phase-controlled regulators, however speed fluctuations may be objectionable and stepless speed control is not possible. Therefore, phase control method offers selective advantages and is desired as a control strategy for SPIMs operation.

The block diagram of the triac-based SPIM drive is illustrated in Fig. 2. Voltage control is accomplished by varying the triac-conducting angle. The two-dimensional magnetic field problem is solved at steady state taking into account the nonlinear magnetic characteristic of stator and rotor cores, as shown in Fig. 3.

The driving functions for the finite element motor model are experimental voltage waveforms obtained with a data acquisition measuring system. Fig. 4 illustrates in a common diagram the sinusoidal voltage with nominal amplitude (dashed curve) and the output voltage of the triac-based controller (solid curve), for a load torque 2 Nm in the 1-hp SPIM. In triac-phase control, the gating signal is delayed so that the device blocks for part of each half-cycle of the supply voltage and thus, fundamental voltage excitation is reduced.

4 Magnetic Field Analysis

Figs. 5 (a) and (b) show the spatial magnetic flux distribution in the 1-hp SPIM with nominal sinusoidal voltage supply and non-sinusoidal voltage of the triac controller respectively, for constant load torque 2 Nm. The magnetic flux distribution of the triac-controlled operation is illustrated in two diagrams, for triac-blocking (at $t = T_S / 5$, where T_S is the time period of the voltage source) and triac-conducting (at $t = 2T_S / 5$). The voltage waveform

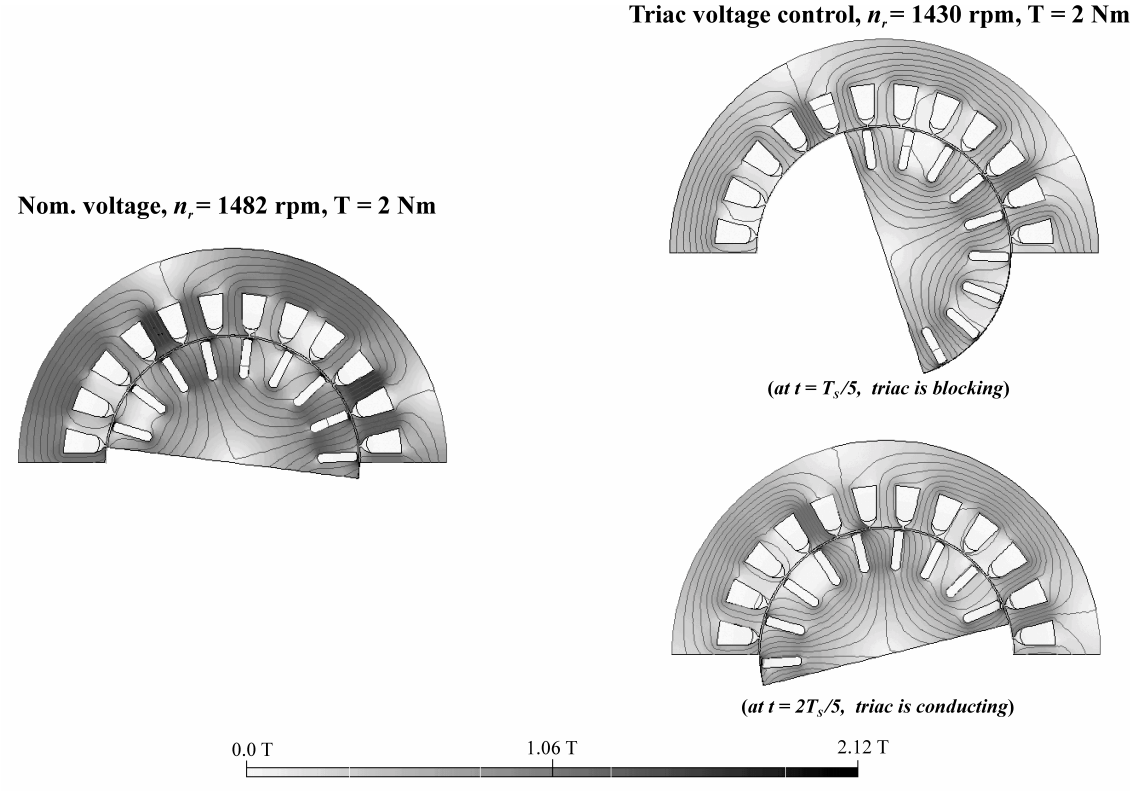

Fig. 5. Flux distribution and equipotential lines in the 1-hp SPIM cross-section, for load torque 2 Nm: (a) nominal voltage and (b) triac-based voltage control.

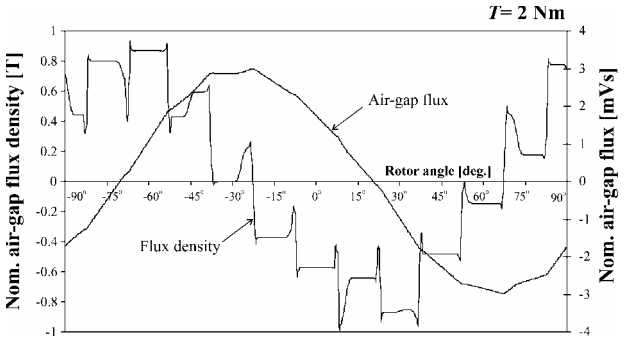

Fig. 6. Air-gap flux density and flux waveforms obtained from finite element analysis, in the 1-hp SPIM with nominal voltage supply.

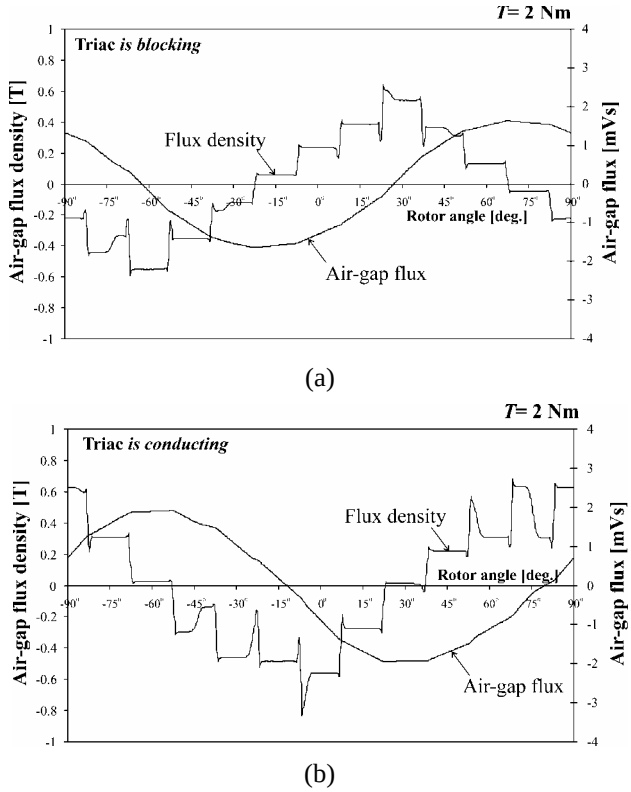

Fig. 7. Air-gap flux density and flux waveforms obtained from finite element analysis, in the 1-hp SPIM with triac controlled voltage supply: (a) triac is blocking and (b) triac is conducting.

for the two modes of triac operation is experimentally obtained (Fig. 4). As shown in Fig. 5, the saturated regions (flux density above 1.5T) are substantially reduced, since the mean supply voltage to the motor is reduced with the triac controller. Thus, the saturation regions are confined in a small portion of the stator and rotor air-gap teeth ends and in the outer end edges of the stator slots.

Figs. 6 and 7 portrays the radial air-gap flux densities and the corresponding air-gap flux profiles obtained through the finite element analysis, for a load torque of 2 Nm. Specifically, Fig. 6 is referred to nominal voltage supply and Figs. 7 (a) and (b) are

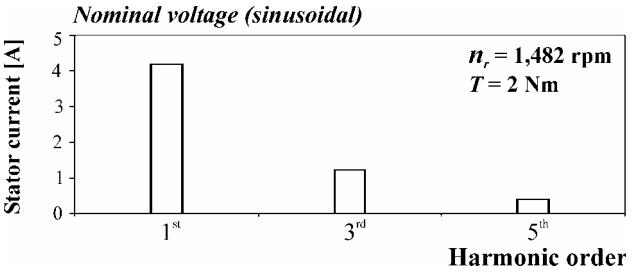

Fig. 8. Harmonic analysis of stator current for nominal (sinusoidal) voltage supply in the 1-hp SPIM, for load torque 2 Nm and speed 1,482 rpm (experimental results).

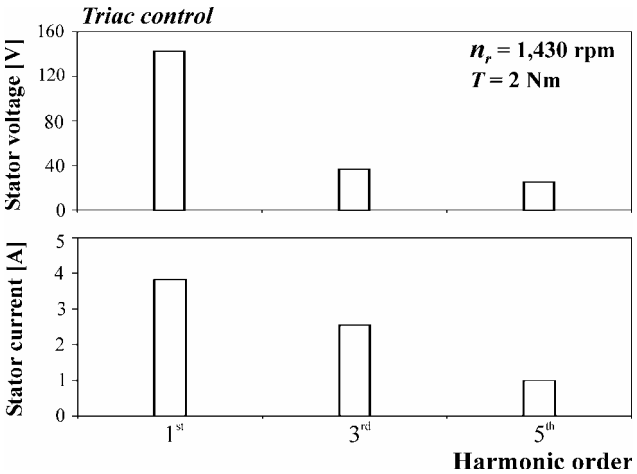

Fig. 9. Harmonic analysis of stator voltage and current for triac control in the 1-hp SPIM, for load torque 2 Nm and speed 1,430 rpm (experimental results).

referred to triac voltage control; specifically, when triac is blocking and conducting respectively. The effect of the slot openings is clearly visible. The maximum values of the nominal and the average triac controlled air-gap flux are 3 mVs and 1.85 mVs respectively. The maximum value of the triac controlled air-gap flux is lower than the nominal by 1.15 mVs. Note that in the triac control, there is a small fluctuation of the maximum values of the air-gap flux, due to switching operation of the triac.

5 Harmonic Analysis

Figs. 8 and 9 illustrate the harmonic analysis of the nominal and triac controlled voltage supply, respectively, of the 1-hp SPIM for a load torque of 2 Nm. It can be seen that triac introduces voltage harmonics and increases stator current harmonics. Consequently, lower power factor values are expected with triac voltage control compared with the nominal stator voltage.

Figs. 10 (a) and (b) illustrate the frequency spectra of the calculated air-gap flux, in dB and linear scale, respectively, with nominal and triac-

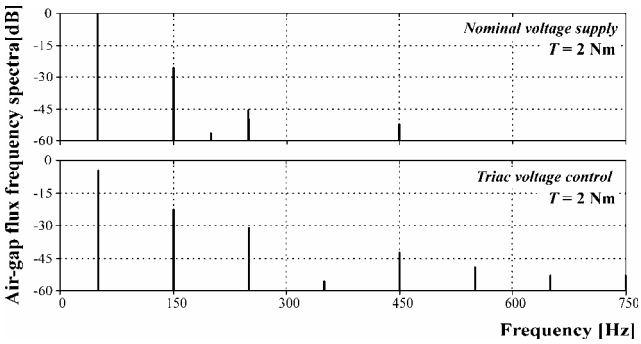

(a)

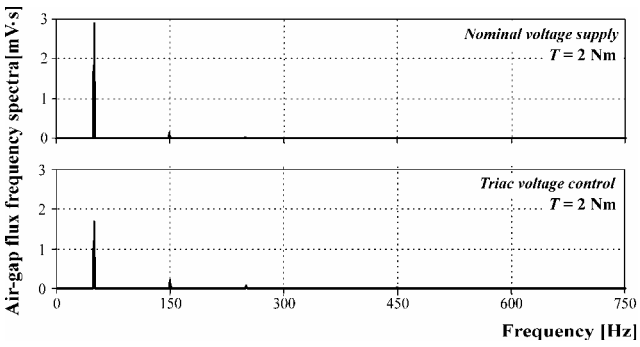

(b)

Fig. 10. Frequency spectra of the calculated air-gap flux with nominal and triac controlled voltage supply, of the 1-hp SPIM for load torque 2 Nm: (a) in dB and (b) linear scale.

controlled voltage, for the case of load torque 2 Nm. For the dB scale, reference flux level is the fundamental flux value of 2.9 mVs. It can be seen that the principal harmonic is the third, at 150 Hz. This is due to magnetic saturation and the non-sinusoidal voltage, for the nominal and triac controlled voltage supply, respectively.

The triac generates high frequency flux harmonics. However, the amplitudes are low compared to the relative higher voltage excitation harmonics, since the amplitudes of the flux harmonics are reduced by the factor $1/h$, where h is the harmonic order. Thus, although the 3rd and 5th order air-gap flux harmonics of the optimal-triac controlled operation are excited by 19.5% and 14% of the nominal supply voltage respectively (Fig. 9), their amplitudes are approximately 6.5% and 2.8% respectively of the nominal air-gap flux fundamental component 2.9 mVs (Fig. 10). Therefore, the magnetic performance of a SPIM is not considerably affected by the triac control.

It should be noted that high performance in SPIM drives could be expected with PWM control techniques (i.e. *V/f* and vector controlled), since the amplitudes of the high carrier-frequency flux harmonics are insignificant. However, a SPIM

coupled with a triac converter offers a far more cost effective drive satisfying most of the commercial and residential applications.

6 Conclusion

In his paper, the magnetic performance of capacitor-run triac voltage controlled SPIM is studied. The magnetic field analysis demonstrates that magnetic saturation is considerably decreased due to the reduced supply voltage, through the triac control. Although triac-based controller introduces voltage and current harmonics, the amplitudes of the flux harmonics are not significant and the magnetic performance of the SPIM is not considerably affected. Selected simulation results are presented obtained through two-dimensional finite element analysis of a SPIM in steady state operation and including the effect of motor rotation.

References:

[1] H. W. Beaty and J. L. Kirtley, *Electric Motor Handbook*, Mc Graw-Hill, 1998.

[2] J. C. Andreas, *Energy - Efficiency Electric Motors*, Marcel Dekker, 2nd edition, 1992.

[3] A. Kaga, Y. Anazawa, and H. Akagami, The Efficiency Improvement of Capacitor Motor with Ferrite Magnetic Wedges, *IEEE Trans. on Magnetics*, vol. MAG-22, no. 5, 1986, pp. 964-966.

[4] H. Huang, E. F. Fuchs, and J. C. White, Optimization of Single-Phase Induction Motor Design, Part II: The Maximum Efficiency and Minimum Cost of an Optimal Design, *IEEE Trans. on Energy Conversion*, vol. 3, no. 2, 1988, pp. 357-366.

[5] L. Xu, Dynamic Model of an Integral-Cycle Controlled Single Phase Induction Machine, *IEEE Trans. on Energy Conversion*, vol. 7, no. 4, 1992, pp. 761-767.

[6] I. Boldea and S.A. Nasar, Unified Analysis of 1-Phase AC Motors Having Capacitors in Auxiliary Windings, *IEEE Trans. on Energy Conversion*, vol. 14, no. 3, 1999, pp. 577-582.

[7] S. Williamson and A.C. Smith, A Unified Approach to the Analysis of Single-Phase Induction Motors, *IEEE Trans. on Industry Applications*, vol. 35, no. 4, 1999, pp. 837-843.

[8] A. C. Reck and L. J. Giacoletto, Simulation of a Motor Control Using Triac Model, *IEEE Trans. on Industry Applications*, vol. 30, no. 5, 1994, pp. 1406-1412.

[9] C. B. Rajanathan and B. J. Watson, Simulation of a Single Phase Induction Motor Operation in the Motoring, Generating and Braking Modes, *IEEE Trans. on Energy Conversion*, vol. 32, no. 3, 1996, pp. 1541-1544.

[10] H. De Gersem, K. De Brabandere, R.J. Belmans, and K. Hameyer, Motional Time-Harmonic Simulation of Slotted Single-Phase Induction Machines, *IEEE Trans. on Energy Conversion*, vol. 17, no. 3, 2002, pp. 313-318.

[11] D. Lin, T. Batan, E.F. Fuchs, and W.M. Grady, Harmonic Losses of Single-Phase Induction Motors under Non-sinusoidal Voltages, *IEEE Trans. on Energy Conversion*, vol. 11, no. 2, 1996, pp. 273-286.

[12] S. Williamson, R.C. Healey, J.D. Lloyd, and J.L. Tevaarwerk, Rotor Cage Anomalies and Unbalanced Magnetic Pull in Single-Phase Induction Motors, *IEEE Trans. on Industry Applications*, vol. 33, no. 6, 1997, pp. 1553-1562.

[13] PC-Opera 2d, Version 9.0, *Rotating Machine* (*RM*) *module*, Oxford, Vector Fields Ltd., 2003.

[14] T. A. Lettenmaier, D.W. Novotny and T.A. Lipo, Single-Phase Induction Motor with an Electrically Controlled Capacitor, *IEEE Trans. on Industry Applications*, vol. 27, no. 1, 1991, pp. 38-43.

[15] T. H. Liu, A Maximum Torque Control with a Controlled Capacitor for a Single-Phase Induction Motor, *IEEE Trans. on Industrial Electronics*, vol. 42, no. 1, 1995, pp. 17-24.

[16] J. M .D. Murphy and F. G. Turnbull, *Power Electronic Control of AC Motors*, Pergamon Press, Oxford, 1988.